A spatial and spectral Analysis of the Sentinel-2 nighttime Image

Merlijn I. Dingemanse[1,*], Daniele Cerra[1], Ferran Gascon[2] and Tobias Storch[1]

[1] German Aerospace Center (DLR), Earth Observation Center (EOC), Münchener Str. 20, 82234 Weßling, Germany
[2] European Space Agency (ESA), European Space Research Institute (ESRIN), Largo Galileo Galilei 1, 00044 Frascati, Italy

Keywords: Sentinel-2, nighttime light, nighttime pyrometry, lighting type detection, EnMAP

Abstract

Nighttime optical remote sensing provides valuable insights into natural and, in particular, human activities. This study evaluates the nighttime imaging capabilities of the Sentinel-2 mission using the only available nighttime acquisition not limited to ocean observations for dark signal calibration, covering the United Arab Emirates with Dubai in 2015. We checked the detection limit using granules over the Persian Gulf, extracted radiance spectra for different regions of interest, and analysed lighting types and temperatures. Results suggest a conservative nighttime detection limit of approx. 0.37 W/m²/μm/sr for visible/near infrared bands, and 0.08 W/m²/μm/sr for short-wave infrared bands. Sentinel-2's high spatial resolution and multispectral bands, although designed for daytime observations, were capable of detecting and classifying bright visible/near and short-wave infrared emitters. Comparisons with hyperspectral EnMAP imagery acquired in 2025 validated the classifications and revealed changes in urban lighting over a decade. While limitations apply, this study highlights S2's potential for nighttime remote sensing and supports considerations of nighttime capabilities for future satellite missions.

1. Introduction

Nighttime optical remote sensing generates valuable indicators of human activities. Visible (VIS) nighttime lights are used for mapping and monitoring human settlements and urban dynamics, estimating demographic and socioeconomic indicators, assessing energy consumption and demand, evaluating natural disasters, and analysing crises and wars (Levin et al., 2020, Cerra et al., 2024). Infrared nighttime data can be used to detect active volcanoes, fires, gas flares and other heavy industry (Elvidge et al., 2013), and monitor conflicts (Dingemanse, 2025). The current state of the art for nighttime remote sensing is the Visible Infrared Imaging Radiometer Suite (VIIRS), installed on three NASA/NOAA satellites. In the VIS range and for nighttime observations, VIIRS offers a single panchromatic day-night-band (DNB) (Miller et al., 2013), which has seen extensive usage in research (Levin et al., 2020, Bennett and Smith, 2017), with a long timeseries and global coverage (Román et al., 2018). VIIRS-DNB is characterized by a high temporal resolution (at least three overpasses per night) and high radiometric sensitivity (2×10^{-7} W/m^2/sr to no saturation). However, VIIRS-DNB also has a low spatial resolution (750 meters) and a broad spectral range (0.5 μm to 0.9 μm). Consequently, VIIRS cannot resolve fine-scale urban structures or discriminate between different types of artificial light sources. Additionally, the late overpass time around 01:30 AM does not match the usual peak of human activities.

Efforts to overcome these limitations have explored alternative data sources: Nighttime photographs taken by astronauts from the International Space Station (ISS) show cities in RGB with varying resolutions (de Miguel et al., 2019, de Miguel et al., 2021), but the images are taken sporadically and are not calibrated. The Jilin-1 satellite captures RGB nighttime imagery at an unparalleled spatial resolution of less than one meter (Guk and Levin, 2020) but only has intermittent coverage. Landsat-8 (LS8) is also capable of capturing nighttime images, with under 100,000 datatakes available. While in the VIS range only the brightest nighttime lights can be detected (Levin and Phinn, 2016), LS8 is very capable of detecting infrared hot sources as small as barbeque fires, outperforming VIIRS in this regard (Wu et al., 2024). Nighttime imagery acquired by the SDGSAT-1 satellite provides high quality observations due to its high spatial and radiometric resolution, as well as a sensor design optimized for low-light conditions. SDGSAT-1 nighttime data has been successfully used to classify lighting types (Jia et al., 2024). In the hyperspectral domain, airborne campaigns with sensors such as AVIRIS were among the first to initiate nighttime data collection (Elvidge and Green, 2005), with (Kruse and Elvidge, 2011) mapping lighting types with a very high spatial resolution. As hyperspectral spaceborne sensors such as EnMAP (Storch et al., 2023) and DESIS (Alonso et al., 2019) became available, it was proven that lighting types over brightly lit cities such as Las Vegas, NV, USA, could be classified using both EnMAP (Bachmann and Storch, 2023, Lind et al., 2024) and DESIS (Ryan et al., 2024). Despite these advances, no dedicated nighttime optical satellite mission currently exists that combines high spatial and spectral resolution with global coverage (Schifano and Hélière, 2025). Understanding how existing satellite missions perform in nighttime conditions is therefore an important intermediate step towards such a mission.

In this context, the Sentinel-2 (S2) mission by the European Space Agency (Drusch et al., 2012) presents a unique situation. S2 provides systematic global coverage using a push-broom sensor with 13 bands spread over the visible (VIS), near and short-wave infrared (NIR and SWIR) ranges, with spatial resolutions of 10, 20, and 60 meters (Gascon et al., 2017). S2's daytime use cases range from land cover use and climate change to disaster monitoring (Phiri et al., 2020). Fire and burnt area detection is also feasible in particular because of S2's two SWIR bands (Hu et al., 2021). Although S2 was not designed for nighttime imaging and nominally acquires the oceans during nighttime every fortnight for dark signal calibration only, a single ad-hoc nighttime acquisition over land was made on 28 September 2015. This datatake has been made available

* Corresponding author. merlijn.dingemanse@dlr.de

to [***] for expert user assessment, presenting the opportunity to analyse S2's capability to capture nighttime data. The aim of this study is to perform a spatial, spectral, and radiometric analysis of S2's nighttime datatake by checking image calibration, locating VIS and infrared emitters, classifying lighting types and estimating temperatures. These aims are achieved by co-registering the datatake, analysing per-band radiances and gathering spectra at specific Regions-Of-Interest (ROIs), which are then matched to existing spectral libraries. These results are then compared to nighttime images of the same ROIs captured by the hyperspectral satellite EnMAP in 2025, ten years later.

The S2 datatake covers much of the United Arab Emirates (UAE), including its capital, Dubai (see Figure 1). In Dubai, several landmarks such as the world's tallest building, Burj Khalifa, are very brightly lit at night. The datatake also includes multiple cement factories with high thermal emissions due to heat generated from production, which can be registered in S2's two SWIR bands. As S2's spatial resolution is comparable to systems such as EnMAP, LS8, and SDGSAT-1, where first nighttime results have been demonstrated, the availability of this datatake offers valuable insights into extending S2's use beyond daytime monitoring. These insights offer new possibilities for cross-sensor studies for nighttime remote sensing.

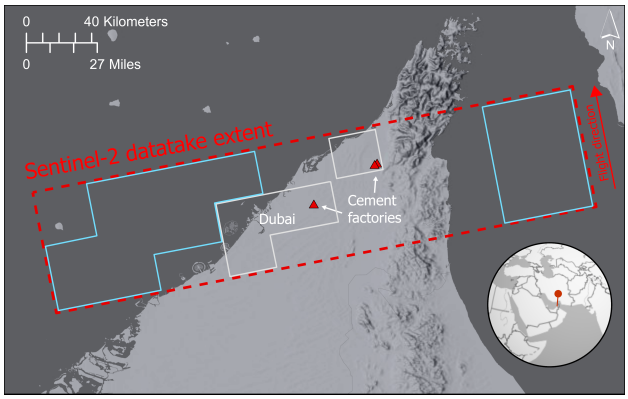

Figure 1. Overview of Sentinel-2's nighttime datatake extent, covering – among others – the brightly lit city of Dubai, UAE, and several cement factories with thermal emissions. Grey boxes show the extent of the analysed granules over land, blue boxes show the extent of water granules used for calculating S2's nighttime detection limits.
(Background map: ArcGIS living atlas)

2. Data and Methods

The chosen approach requires selected granules of the S2 nighttime datatake, lighting and temperature spectra and EnMAP imagery. Outputs are georeferenced images, as well as lighting and temperature spectra for specified ROIs. An overview of the data and methods is illustrated in Figure 2.

2.1 Lighting and Temperature Spectra

The lighting spectra required for lighting type detection were taken from (Elvidge et al., 2010), who provides spectra for various lighting types as measured in a laboratory. All these spectra were collected in the wavelength range between 350 nm and 2500 nm at a fine spectral resolution of 1 nm, covering lighting emissions in VIS/NIR and SWIR. Considered lighting types include LED, high-pressure sodium, low-pressure sodium, fluorescent, ceramic metal halide, xenon, incandescent and kerosine

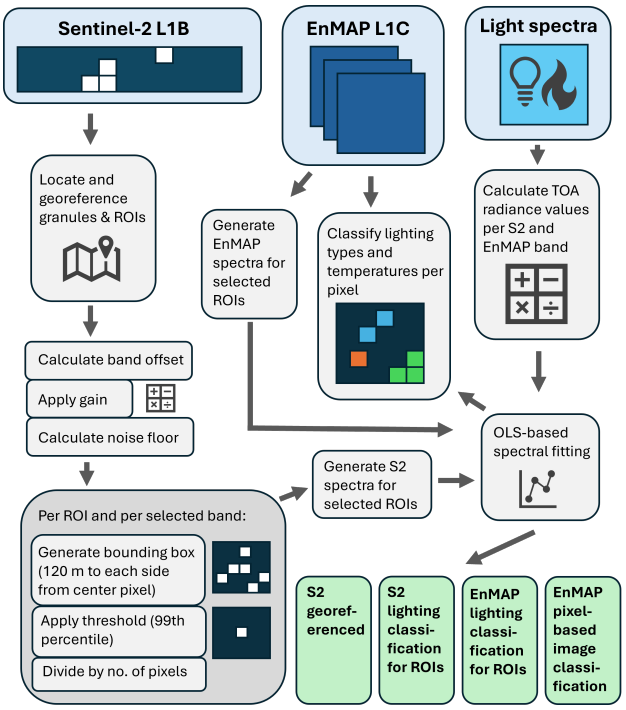

Figure 2. Approach taken in this study. Blue tiles illustrate inputs, grey tiles illustrate processing steps, green tiles illustrate outputs.

lamps, covering most of illumination sources present in modern cities. From the spectral library, we picked 24 spectra, representing and balancing the number of spectra for the different lighting types. Kerosine lamps are not considered here because their spectrum is too similar to a thermal emission at approx. 1310 K (if pressurized) and 2050 K (if liquid), and therefore, considered as a thermal event. Additionally, 201 temperature radiances according to Planck's law and ranging from 500 K to 2500 K in steps of 10 K were generated. As incandescent lamps have a spectrum similar to a thermal emission at approx. 3195 K, this was considered as a lighting type. All spectra were then transformed into S2's at-sensor radiances L_{band} for each band accounting for its spectral response function using the following formula:

$$L_{\text{band}} = \frac{\sum_\lambda \left(L_{\text{light/temp}}(\lambda) \cdot T_{\text{atm}}(\lambda) \cdot R_{\text{band}}(\lambda) \right)}{\sum_\lambda R_{\text{band}}(\lambda)} \quad (1)$$

where:

$L_{\text{light/temp}}(\lambda)$ lighting type or thermal emission at wavelength λ
$T_{\text{atm}}(\lambda)$ atmospheric transmission at wavelength λ (considers factor $1/\cos(\alpha)$ for observation tilt of α)
$R_{\text{band}}(\lambda)$ spectral response function of band at wavelength λ

For atmospheric transmission, a standard atmosphere was considered. Thus, L_{band} describes the expected radiance per lighting or temperature spectrum measured in each S2 band. Lastly, L_{band} was normalized as:

$$L_{\text{norm,band}} = \frac{L_{\text{band}}}{\sum_{\text{band}} L_{\text{band}}} \quad (2)$$

whereby only the ten bands at 10 meter and 20 meter ground sampling distance were considered. The 60 meter bands were removed due to their focus on atmospheric parameters and comparatively low resolution.

2.2 Sentinel-2

The S2 datatake is processed to Level-1B Top-Of-Atmosphere (TOA), meaning that radiometric corrections have been applied, but the image has not been orthorectified or geolocated (Gascon et al., 2017). This processing level provides imagery in 25×23 km^2 granules of single bands covering the swath of 290 km, which cannot be easily co-registered due to a small offset in the capture time for each band. Also, the imagery contains digital numbers, which require the application of a different gain factor for each band to estimate radiances. As such, several methods have to be applied to derive comparable radiances for the ROIs.

Satellite	Sentinel-2A	EnMAP
Date and time of capture (local)	2015-09-28, 22:31	2025-09-13, 23:01 2025-09-21, 23:09 2025-10-10, 23:02
Product type	Level-1B	Level-1C

Table 1. Properties of Sentinel-2 and EnMAP data used in the study.

First, the granule footprint of each of the 36 granules was located using the datatake's metadata. Each band was divided by its respective band gain, and detection limits were estimated by calculating the mean and standard deviation (stdev) for all pixels of the 15 granules, that were located in their entirety over water (see Figure 3). Next, selected granules containing ROIs such as the city of Dubai and cement factory locations were then roughly co-registered using single VIS and SWIR bands in Google Earth Pro to identify objects with the strongest VIS and SWIR emissions.

For the considered spectral bands, a pixel-based spatial offset was first calculated per granule using the relative position of center pixels of ROIs with high radiances in all bands. This approach allowed for the automatic selection of center pixel coordinates for each ROI using just the center pixel of B2 (VIS ROIs) or B12 (SWIR ROIs). For each ROI, a bounding box of 120 meters around the center pixel was extracted per band. This boundary box approach and specific box size was chosen to minimize co-registration errors and to ensure that a comparable area was extracted regardless of band resolution. Next, only pixels at or above the 99$^{\text{th}}$ percentile within the bounding box were selected. This was done to ensure the brightest pixels were not averaged out by the large number of low-radiance pixels present within each bounding box. These pixels were then averaged, with the resulting output being a radiance value [W/m²/sr/μm] for each band for each ROI. Each spectrum was then normalized and matched to the previously described normalized spectral library of lighting types and temperatures using the Ordinary Least Squares method (OLS):

$$\sum_{\text{band}} (L_{\text{norm, band}} - S_{\text{norm, band}})^2 \tag{3}$$

where:

$L_{\text{norm, band}}$ normalized reference spectrum value at each band
$S_{\text{norm, band}}$ normalized measured spectrum value at each band

Using OLS, it is only possible to identify the dominant lighting type or temperature. As such, lighting and temperature mixtures are not considered. As all spectra were normalized, this approach is similar to the Spectral Angle Mapper approach, as it mainly relies on the shape of the spectra. Reflected light by moon illumination was not considered, as the total emitted TOA lunar radiance in the considered spectral range lies several orders of magnitude below the calculated S2 detection limit (Kieffer and Stone, 2005). Lastly, results were compared to a similar classification based on EnMAP data.

2.3 EnMAP

EnMAP (Environmental Mapping and Analysis Program) is a high-resolution imaging spectroscopy mission operational since 2 November 2022 (Storch et al., 2023). The satellite features continuous coverage in for the range 0.42 µm to 2.45 µm in 224 narrow spectral bands, a spatial resolution of 30 m, and a swath width of 30 km. EnMAP acquisitions are tasking-based rather than systematic, allowing flexible image capture, including the acquisition of nighttime imagery during ascending orbits. Following a method by (Bachmann and Storch, 2023), three Level-1C EnMAP datatakes, namely orthorectified TOA radiances, over Dubai were analysed (see Table 1). To avoid strong atmospheric absorption regions, selected spectral ranges were used, namely: 0.42–0.9 µm (78 bands), 1.0–1.1 µm and 1.175–1.3 µm (20 bands), 1.5–1.725 µm (20 bands), and 2.105–2.275 µm (20 bands). Next, convolved sRGB and pan-thermal composites were created by summing relevant bands and applying an appropriate linear scaling factor.

To estimate the detection limit, we considered more than 250.000 pixel for each band over the (dark) Persian Gulf and derived an average of below 0.018 W/m²/sr/µm and a stdev of below 0.025 for all considered bands (see Figure 3). The expected changes in the sensitivity of the detector in VIS/NIR, namely a higher sensitivity for wavelength at 0.69 μm, and in particular the change from low-gain to high-gain for the last 20 bands in SWIR are clearly visible. Note that being broad, single S2 bands cannot be directly compared to single EnMAP bands.

Next, EnMAP spectra were taken from selected ROI's and matched to lighting and thermal spectra as performed with S2 spectra. As Level-1C products are co-registered, a pixel-based lighting type classification and temperature estimation was then performed on the entire image. For the classification of lighting types, pixels are only considered if the radiance associated with scotopic vision (Donatello et al., 2019), which corresponds to human vision under low-light conditions, is at least 3 W/m²/sr/µm. For temperatures, a detection is triggered if the thermal emission, namely $\sigma \epsilon T^4$, where $\sigma = 5.67 \times 10^{-8}$ W/m²/K^4 (Stefan–Boltzmann constant) and ϵ the estimated pixel fraction covered by the thermal emission calculated at a temperature of T K, is at least 0.6 W/m².

For this step, individual lighting types within each category were merged to reduce class complexity. Lastly, EnMAP spectra for selected ROIs also covered by S2 were transformed into simulated S2 bands, allowing for better comparison.

3. Results

3.1 Detection Limit

Results from the 15 tiles completely covered by water show mean radiance to be below 0.06 W/m²/sr/µm, and stdev to be below 0.11 for all VIS/NIR bands (see Figure 3). In the SWIR range, mean radiance is below 0.02 W/m²/sr/µm and stdev is below 0.02. When applying the standard formula of mean + 3 × stdev, a conservative detection limit of approx. 0.37 W/m²/sr/µm per band in the VIS/NIR can thus be assumed, which is comparable to LS8 (Levin and Phinn, 2016). In the SWIR range, a detection limit of approx. 0.08 W/m²/sr/µm can be assumed. Compared to EnMAP, convolving the EnMAP bands to S2 bands, results in mean + 3 × stdev of below 0.03 W/m²/sr/µm, and considering the spatial resolution results in values of below 0.05 for the S2's 10 m and 0.04 for S2's 20 m bands, that is by a factor of at least eight lower than for S2 itself.

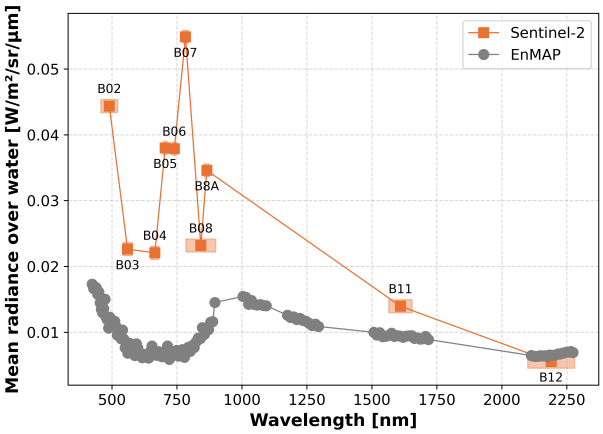

Figure 3. Comparison of per-band mean radiance values over dark water for Sentinel-2 (orange) and the selected EnMAP bands (grey). Orange boxes illustrate S2's spectral coverage.

3.2 Spatial Analysis

The results of S2 co-registration is shown in Figure 5, which compares a S2 daytime image of downtown Dubai against a nighttime panchromatic composite of VIS/NIR bands. The layout of Dubai's commerce centers can be here established from the nighttime image alone, with Burj Park, the World Trade Centre, the Dubai International Financial Centre, and a large retail street all detectable. In contrast, Dubai's residential areas show little to no emissions, apparently lying well below the detection threshold of S2's bands. A string of individual bright objects such as mosques also makes it possible to estimate the coastline's position in the image due to a complete absence of emissions over water. Due to high radiance in some areas, it is also possible to identify the individual buildings and regions responsible for the largest radiances. The brightest objects in the city of Dubai are the Burj Khalifa, the fountains in Burj Park, as well as several other skyscrapers, the shape of which can be identified due to S2's relatively high spatial resolution of 10 meters.

A comparison with EnMAP nighttime imagery confirms the correct georeferencing of the S2 nighttime granules (see Figure 4). EnMAP, with its lower detection limits, is capable of detecting more of the cities' lighting, with main roads and most of the larger buildings clearly visible. The ten-year time gap between the S2 and EnMAP imagery also allows for change detection. Dubai has undergone significant development since 2015, meaning that new nighttime lights appeared. This is most clearly visible in the Bay Square and Business Bay surrounding the Burj Khalifa, where a large number of skyscrapers have since been constructed (see Figure 4). Given their powerful lighting, they should have been visible in the S2 nighttime imagery if they had been constructed yet despite S2's lower sensitivity. This can most clearly be seen for the Damac towers. These towers were seen to be under construction in 2015 (see Figure 4b) and were finished around 2018 (see Figure 4d), with strong emissions visible in EnMAP, but not in S2. In the opposite case, the Burj Park fountains underwent maintenance from May 2025 to October 2025 and are thus visible in S2, but not in EnMAP.

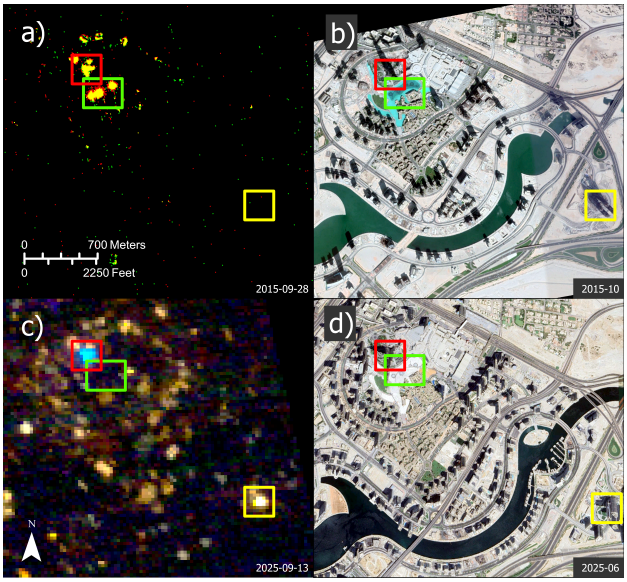

Figure 4. Comparison between an Sentinel-2 RGB nighttime image (a) and an EnMAP convolved nighttime sRGB image (c). High-resolution imagery over the ROI in 2015 (b) and 2025 (d) is shown. The location of the Burj Khalifa is highlighted in red, the Damac towers are highlighted in yellow, and the Burj Park fountains are highlighted in green.
(a. © Copernicus Sentinel data 2015, b. and d. Google Earth Pro, c. EnMAP data © DLR 2025. All rights reserved)

3.3 Lighting Type Detection

The results of the lighting type detection are shown in Figure 6, where five spectra of bright ROIs are depicted. S2 appears capable of differentiating between lighting types, with large structures' lighting being classified as xenon and ceramic metal halide, while an industrial hall is identified as LED. The Burj Khalifa, which was known to be lit by xenon lights and a large LED screen (Flash Technology, 2010, Hondel Lighting, 2023) in 2015, is correctly classified as xenon. Due to their spectral similarity concerning S2, the xenon and ceramic metal halide lighting types also have very similar OLS residuals, leading to possible incorrect classifications.

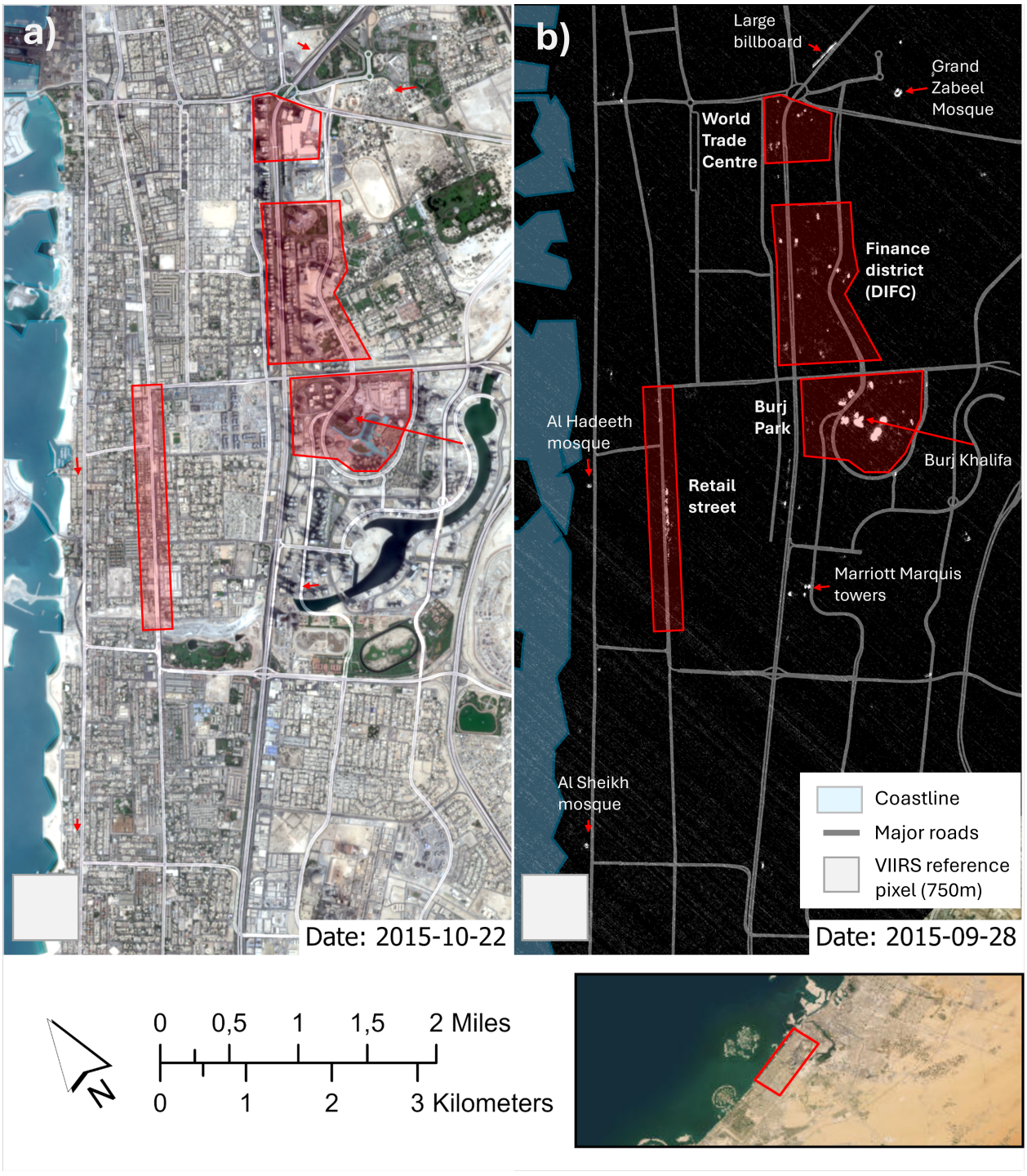

Figure 5. Inter-comparison of a daytime Sentinel-2 RGB image (a) and the nighttime Sentinel-2 image (b) displayed as a panchromatic VIS/NIR composite (bands 2,3,4,8 with linear stretch applied). Visible city structures and individual bright objects are marked in red. (ArcGIS living atlas, © Copernicus Sentinel data 2015, OpenStreetMap)

Despite the time gap of ten years, the results match well with EnMAP's classification. For many ROIs the lighting type detected by S2 is also one of the dominant lighting types in EnMAP, with others shifting to LED. As the classification is pixel-based, EnMAP allows different lighting types per ROI, which is more realistic. In EnMAP, the Burj Khalifa contains accurately classified pixels of both LED and xenon. The NAS sports complex stadium is classified as a combination of xenon and metal halide. Concerning the spectra of the Burj Khalifa, the spectral matching of both S2 and EnMAP is less adequate, with a large emission peak around 700 nm (S2 band 4), and no noticeable peak at 800 nm to 900 nm (S2 band 8) in measured spectra.

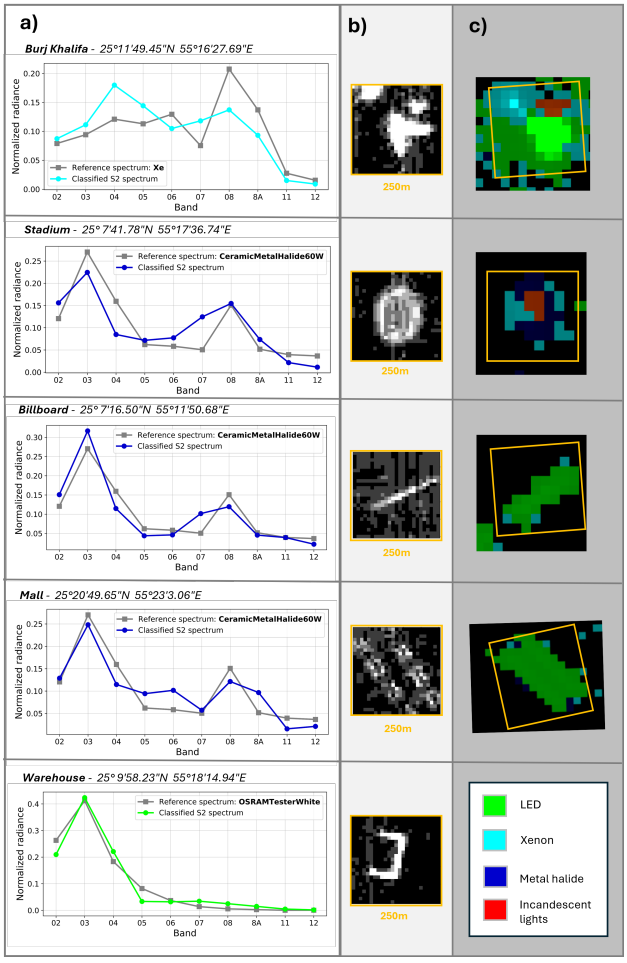

Figure 6. Inter-comparison of Sentinel-2- and EnMAP-based lighting type classification of the ROIs. a) shows Sentinel-2 classifications for entire ROIs using the bounding box seen in b). c) shows per-pixel EnMAP classification for the entire ROIs, where orange boxes inside the EnMAP classifications show the approximate footprint of the Sentinel-2 bounding box. ROI coordinates are noted above the spectra. The bottom spectrum (warehouse) fell outside of EnMAP's coverage.
(b. © Copernicus Sentinel data 2015, c. EnMAP data © DLR 2025. All rights reserved)

However, as all other lighting types show good spectral fits, and both the S2 spectrum and the EnMAP spectra of xenon in this ROI are similar to one another, a measurement error seems unlikely. Due to the complexity of Burj Khalifa's lighting and the limited number of xenon spectra in the reference spectral library, it is likely that the signal comes from multiple lighting types, some of which might not be adequately covered by our dataset. In terms of change detection, most lighting sources in the 2025 EnMAP classification are classified as LED. This result is plausible as worldwide LED usage has vastly increased since 2015 (Zissis et al., 2021). A spectral comparison of the Souq Park Mall as well as a large billboard between 2015 and 2025 also shows this shift, with S2 classifying both ROIs as ceramic metal halide, while EnMAP classifies them as LED. S2 nighttime data can thus provide information on the changes in how cities are lit.

3.4 Pyrometry

The two large cement factories present in the S2 datatake both show very high radiances in the B11 and B12 SWIR bands. As seen in Figure 7, the temperature curves with the best fit were 940 K and 820 K respectively. These results are close to the calculated mean temperature of 955 K for cement emitters found in the VIIRS Nightfire (VNF) permanent emitter database (Elvidge et al., 2013), with many cement emitters in the 800 K to 950 K range. In addition, the two cement factories are not actually listed in the VNF permanent emitter database, presumably because they remained undetected by VIIRS. As such, S2 can detect hot sources at night that were missed by VIIRS, similar to LS8 (Wu et al., 2024).

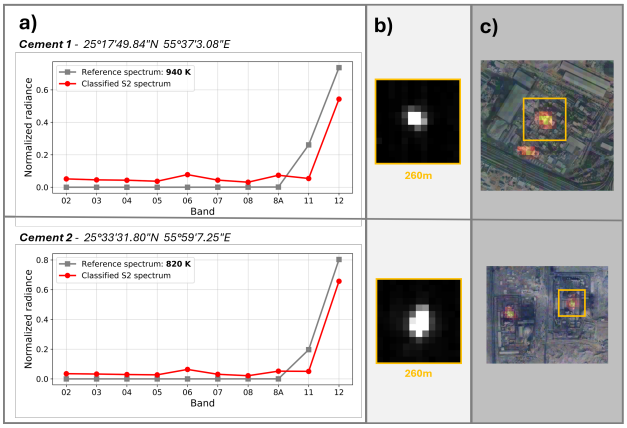

Figure 7. Comparison between cement factory hot sources in Sentinel-2 and EnMAP. a) shows calculated temperatures for the bounding box. b) shows the B12 SWIR. c) shows per-pixel classified hot sources from EnMAP overlaid on top of imagery by Google Earth Pro, where the orange boxes in show the approximate location of the Sentinel-2 bounding boxes.
(b. © Copernicus Sentinel data 2015, c. Google Earth Pro and EnMAP data © DLR 2025. All rights reserved)

A comparison with EnMAP ten years later shows that both cement factories are still active. However, per-pixel classifications vary quite substantially compared to those calculated by S2. EnMAP pixel temperatures range between 600 K and 1000 K, with several pixels with small signals being misclassified as temperatures above 2000 K. Additionally, EnMAP is capable of detecting SWIR emissions in two more structures in one of the cement factories. These results highlight the value of S2-based analysis of high-temperature events for tracking industrial activity at night.

4. Discussion

4.1 Limits in Approach

Several limits in approach apply. For S2, co-registration accuracy and selection of spectral sampling areas were only approximate. This issue could be resolved if Level-1C products were available. Next, the results for lighting type classification vary greatly depending on the threshold method chosen. Our high detection limit and focus on bright pixels delivers good results, but also masks out smaller radiances. For both S2 and EnMAP lighting type detection, no reliable validation data was available. While the results are strengthened by cross-validation between the two satellites, this limits interpretability. Additionally, the approach does not allow for different lighting types within a single pixel. In the future, spectral unmixing approaches could be applied to account for this limitation. For pyrometry, hot sources have negligible emissions in the VIS/NIR range, meaning that only two bands can be used to estimate the slope of the Planck curve for S2. Despite these limitations, the results still provide a useful indication of lighting and thermal activity patterns.

4.2 Sentinel-2's Nighttime Capabilities in Context

Based on the results presented in this study, we can now compare how S2's nighttime capabilities perform in comparison to other missions. Compared to VIIRS-DNB (Miller et al., 2013), only the brightest VIS/NIR objects can be detected due to a much higher detection limit. However, S2's better spatial and spectral resolution mean that VIS/NIR emitters can be located much more accurately. In the SWIR range, S2 is also capable of detecting hot sources that might not be detectable in VIIRS' large footprint. Additionally, S2's overpass time is much earlier in the night compared to VIIRS, allowing for the monitoring of nighttime lights in the late evening instead of the middle of the night. Compared to LS8, S2 delivers similar results and has a similar detection threshold in VIS/NIR (Levin and Phinn, 2016), although S2's spatial resolution is higher (10 m compared to 30 m). In the SWIR range, LS8 data can be plausibly used to detect hot sources as small as grill fires (Wu et al., 2024). Investigating if this would also be possible with S2 would require additional validation data. LS8 also comes equipped with two long-wave infrared (LWIR) bands, with which normal temperatures can be monitored. SDGSAT-1's VIS/NIR images have a much higher sensitivity than S2 (Guo et al., 2023), but the satellite lacks SWIR bands, making pyrometry not feasible. The optimization of the configuration of bands for the detection of lighting types is investigated in (de Meester and Storch, 2020). Finally, compared to EnMAP, which provides superior spectral information as well as better radiometric performance in the VIS/NIR range, S2's main advantages are its larger swath size and potential for continuous monitoring, because of the higher temporal resolution. However, this benefit only applies if such frequent observations during nighttime are actually performed.

5. Conclusion

This study set out to perform a spatial and spectral analysis of S2's only nighttime datatake over land, and to compare the results to observations from the imaging spectroscopy mission EnMAP. Results show that a conservative detection limit of approximately 0.37 W/m²/sr/µm in the VIS/NIR and 0.08 W/m²/sr/µm in the SWIR range can be assumed for S2. Results also show that it is not only possible to detect bright VIS/NIR and SWIR objects, but also to classify lighting types and temperatures, although limits apply. Classifications were validated against EnMAP imagery acquired ten years later, which nevertheless showed good agreement in classification results for selected ROIs, and also showed how Dubai's lighting has changed between 2015 and 2025. Improvements include better co-registration for which S2 Level-1C products would be required. S2's nighttime capabilities match LS8's, where first results have been achieved using nighttime data from both VIS/NIR and SWIR bands. As such, S2's potential to capture nighttime imagery should be further explored, and considered when specifying future missions. For Sentinel-2's future, Sentinel-2 Next-Generation, regular nighttime acquisitions are planned (Patterson and Reina, 2025).

Author contributions

Conceptualization, T.S. and M.D.; methodology, M.D, T.S. and D.C.; software, M.D. and T.S.; data curation, F.G.; formal analysis, M.D. and T.S.; writing—original draft, M.D.; writing—review and editing, T.S., D.C. and F.G.; visualization, M.D.; supervision, T.S. All authors have read and agreed to the published version of the manuscript.

References

Alonso, K., Bachmann, M., Burch, K., Carmona, E., Cerra, D., ..., Tegler, M., 2019. Data Products, Quality and Validation of the DLR Earth Sensing Imaging Spectrometer (DESIS). *Sensors*, 19(20), 4471.

Bachmann, M., Storch, T., 2023. First Nighttime Light Spectra by Satellite—By EnMAP. *Remote Sensing*, 15(16), 4025.

Bennett, M. M., Smith, L. C., 2017. Advances in using multitemporal night-time lights satellite imagery to detect, estimate, and monitor socioeconomic dynamics. *Remote Sensing of Environment*, 192, 176-197.

Cerra, D., Merkle, N., Henry, C., Gapp, S., Gstaiger, V., 2024. Increases in Night Lights Intensity Reveal Extreme Events: A Case of Study on the Ongoing Conflict in Ukraine. *ISPRS Annals of the Photogrammetry, Remote Sensing and Spatial Information Sciences*, X-3-2024, 53-59.

de Meester, J., Storch, T., 2020. Optimized performance parameters for nighttime multispectral satellite imagery to analyze lightings in urban areas. *Sensors*, 20(11), 3313.

de Miguel, A. S., Kyba, C. C., Aubé, M., Zamorano, J., Cardiel, N., ..., Gaston, K. J., 2019. Colour remote sensing of the impact of artificial light at night (I): The potential of the International Space Station and other DSLR-based platforms. *Remote Sensing of Environment*, 224, 92-103.

de Miguel, A. S., Zamorano, J., Aubé, M., Bennie, J., Gallego, J., ..., Gaston, K. J., 2021. Colour remote sensing of the impact of artificial light at night (II): Calibration of DSLR-based images from the International Space Station. *Remote Sensing of Environment*, 264, 112611.

Dingemanse, M., 2025. Towards conflict monitoring with viirs nighttime data: The war in ukraine. Master's thesis, University of Stockholm.

Donatello, S., Rodríguez, R., Quintero, M. G. C., Wolf, O., Van Tichelen, P., ..., Hoof, T. G., 2019. Revision of the EU green public procurement criteria for road lighting and traffic signals. *Publications Office of the European Union: Luxembourg*, 127.

Drusch, M., Del Bello, U., Carlier, S., Colin, O., Fernandez, V., ..., Bargellini, P., 2012. Sentinel-2: ESA's Optical High-Resolution Mission for GMES Operational Services. *Remote Sensing of Environment*, 120, 25-36.

Elvidge, C. D., Green, R. O., 2005. *High- and low-altitude AVIRIS observations of nocturnal lighting*. Pasadena, CA: Jet Propulsion Laboratory, National Aeronautics and Space Agency.

Elvidge, C. D., Keith, D. M., Tuttle, B. T., Baugh, K. E., 2010. Spectral identification of lighting type and character. *Sensors*, 10(4), 3961-3988.

Elvidge, C. D., Zhizhin, M., Hsu, F.-C., Baugh, K. E., 2013. VIIRS Nightfire: Satellite Pyrometry at Night. *Remote Sensing*, 5(9), 4423-4449.

Flash Technology, 2010. Burj Khalifa – Dubai, United Arab Emirates. `https://www.flashtechnology.com/burj-khalifa/`. Accessed: 2025-10-31.

Gascon, F., Bouzinac, C., Thépaut, O., Jung, M., Francesconi, B., ..., Fernandez, V., 2017. Copernicus Sentinel-2A Calibration and Products Validation Status. *Remote Sensing*, 9(6), 584.

Guk, E., Levin, N., 2020. Analyzing spatial variability in nighttime lights using a high spatial resolution color Jilin-1 image – Jerusalem as a case study. *ISPRS Journal of Photogrammetry and Remote Sensing*, 163, 121-136.

Guo, H., Dou, C., Chen, H., Liu, J., Fu, B., ..., Liang, D., 2023. SDGSAT-1: the world's first scientific satellite for sustainable development goals. *Science Bulletin*, 68(1), 34-38.

Hondel Lighting, 2023. How Burj Khalifa Lighting Works? `https://hondellighting.com/burj-khalifa.html`. Accessed: 2025-10-31.

Hu, X., Ban, Y., Nascetti, A., 2021. Sentinel-2 MSI data for active fire detection in major fire-prone biomes: A multi-criteria approach. *International Journal of Applied Earth Observation and Geoinformation*, 101, 102347.

Jia, M., Zeng, H., Chen, Z., Wang, Z., Ren, C., ..., Wang, Y., 2024. Nighttime light in China's coastal zone: The type classification approach using SDGSAT-1 Glimmer Imager. *Remote Sensing of Environment*, 305, 114104.

Kieffer, H. H., Stone, T. C., 2005. The Spectral Irradiance of the Moon. *The Astronomical Journal*, 129(6), 2887.

Kruse, F. A., Elvidge, C. D., 2011. Identifying and mapping night lights using imaging spectrometry. *2011 Aerospace Conference*, IEEE, 1–6.

Levin, N., Kyba, C. C., Zhang, Q., Sánchez de Miguel, A., Román, M. O., ..., Elvidge, C. D., 2020. Remote sensing of night lights: A review and an outlook for the future. *Remote Sensing of Environment*, 237, 111443.

Levin, N., Phinn, S., 2016. Illuminating the capabilities of Landsat 8 for mapping night lights. *Remote Sensing of Environment*, 182, 27-38.

Lind, L., Cerra, D., Pato, M., Pölönen, I., 2024. Analyzing artificial nighttime lighting using hyperspectral data from enmap. *International Geoscience and Remote Sensing Symposium 2024 (IGARSS)*, IEEE, 8069–8073.

Miller, S. D., Straka, W., Mills, S. P., Elvidge, C. D., Lee, T. F., ..., Weiss, S. C., 2013. Illuminating the Capabilities of the Suomi National Polar-Orbiting Partnership (NPP) Visible Infrared Imaging Radiometer Suite (VIIRS) Day/Night Band. *Remote Sensing*, 5(12), 6717-6766.

Patterson, J., Reina, F., 2025. Sentinel-2 Mission Status and Outlook: Sentinel-2 Next Generation. *ESA Living Planet Symposium*.

Phiri, D., Simwanda, M., Salekin, S., Nyirenda, V. R., Murayama, Y., Ranagalage, M., 2020. Sentinel-2 Data for Land Cover/Use Mapping: A Review. *Remote Sensing*, 12(14), 2291.

Román, M. O., Wang, Z., Sun, Q., Kalb, V., Miller, S. D., ..., Masuoka, E. J., 2018. NASA's Black Marble nighttime lights product suite. *Remote Sensing of Environment*, 210, 113-143.

Ryan, R. E., Pagnutti, M., Ryan, H., Burch, K., Manriquez, K., 2024. Satellite Hyperspectral Nighttime Light Observation and Identification with DESIS. *Remote Sensing*, 16(5), 923.

Schifano, L., Hélière, A., 2025. Advancements and challenges in nighttime light remote sensing. *International Conference on Space Optics 2024 (ICSO)*, SPIE, 136992F.

Storch, T., Honold, H.-P., Chabrillat, S., Habermeyer, M., Tucker, P., ..., Fischer, S., 2023. The EnMAP imaging spectroscopy mission towards operations. *Remote Sensing of Environment*, 294, 113632.

Wu, H., Liu, Y., Pu, Y., Liu, P., Zhao, W., Guo, X., 2024. National-scale nighttime high-temperature anomalies from Landsat-8 OLI images. *ISPRS Journal of Photogrammetry and Remote Sensing*, 212, 212-229.

Zissis, G., Bertoldi, P., Serrenho, T., 2021. Update on the status of LED-lighting world market since 2018. EUR Report EUR 30500 EN, Publications Office of the European Union, Luxembourg.